Journal of Electromagnetic Waves and Applications

ISSN: 0920-5071 (Print) 1569-3937 (Online) Journal homepage: http://www.tandfonline.com/loi/tewa20

Extracting Volterra series representation from *X*-parameters for the modeling of microwave device

L. Sang , J. Wang , Y. Xu & R. Xu

To cite this article: L. Sang , J. Wang , Y. Xu & R. Xu (2013) Extracting Volterra series representation from *X*-parameters for the modeling of microwave device, Journal of Electromagnetic Waves and Applications, 27:3, 299-308, DOI: 10.1080/09205071.2013.744283

To link to this article: https://doi.org/10.1080/09205071.2013.744283

Published online: 19 Nov 2012.

Journal of Electromagnetic Waves and Applications, 2013
Vol. 27, No. 3, 299–308, http://dx.doi.org/10.1080/09205071.2013.744283

Taylor & Francis
Taylor & Francis Group

Extracting Volterra series representation from *X*-parameters for the modeling of microwave device

L. Sang*, J. Wang, Y. Xu and R. Xu

Fundamental Science on EHF Laboratory, University of Electronic Science and Technology, Chengdu, China

(*Received 31 August 2012; accepted 10 October 2012*)

As a classic mathematical means, Volterra series are good representations for the description of nonlinear microwave devices and systems. However, the difficulty in extracting accurate kernel functions is the most important reason that limits wider application of Volterra series. In this research, the *X*-parameters proposed in recent years are used to resolve this problem for the first time. The extraction method is detailed, and the results show that it is very convenient to obtain Volterra series representation by using *X*-parameters. A power amplifier was measured to verify the proposed approach, and a good agreement has been achieved between the measured results and the predicted data based on the Volterra series. The method proposed in this paper is useful for accurate and fast modeling of modern microwave devices.

1. Introduction

Behavioral modeling of microwave components is of great interest to the designers of microwave devices used in today's wireless systems. In the past several decades, scattering parameters (*S*-parameters) have contributed greatly to the modeling of linear microwave devices [1,2]. However, a big problem still disturbing engineers is the absence of an efficiency way, which can easily characterize, describe mathematically, and simulate the nonlinear behavior of microwave components accurately. A lot of mathematical equations and methods have been brought forward to describe the nonlinear characterization. As one of the most popular expressions for nonlinear systems [3], Volterra series have been used in many weakly nonlinear applications. However, there are still two disadvantages need to be overcome for wider application in the modeling of microwave devices. One is that the contribution of each frequency component in the stimuli to response should be distinguished clearly, which is not very convenient. The other one is that it involves a large amount of testing work especially for multi-tone stimuli. If the order is over 3rd, the testing work can hardly be completed by general testing equipments.

The advent of the Poly-Harmonic Distortion (PHD) nonlinear behavioral model and its *X*-parameters proposed in recent years brings great convenience to the use of Volterra series [4,5]. The *X*-parameters, which can be obtained easily from modern Nonlinear Vector Network Analyzer (NVNA), are the natural extension of *S*-parameters to nonlinear devices. The *X*-parameters framework not only greatly simplifies the testing workload, but also

*Corresponding author. Email: sanglei2008@126.com

describes all of the numerical relationships of every frequency component (fundamental frequency, harmonic frequency, and inter-modulated frequency) at each port of the device. In this paper, a weakly nonlinear power amplifier module was measured by the NVNA, and *X*-parameters were used as the basic data to extract the kernel functions of the Voterra series in frequency domain for the first time. Then the kernel functions in time domain and the integrated Volterra series expression could be achieved. The output performance of the power amplifier could be calculated and predicted by using Volterra series expression. The results show that it is very convenient to obtain Volterra series by using *X*-parameters and the predicted results based on this Volterra series agree well with the measured data.

2. Brief description of the *X*-parameters

The fundamentals of PHD modeling are introduced and described in [4,5]. The PHD modeling is a black-box, frequency-domain modeling technique initially developed for nonlinear microwave components and systems. The PHD model is empirically extracted by exciting a nonlinear Device Under Test (DUT) with external signals and measuring the response at the desired port. The PHD formulation states that for a given DUT there is a set of multivariate nonlinear functions F_{pm} that relates all the input components A_{qn} with the output components B_{pm}, where q and p range from one to the number of network port Q and m and n range from zero up to the highest harmonic order N. This is formally expressed as:

$$B_{pm} = F_{pm}\left(A_{11}, A_{12}, \ldots, A_{1N}, \ldots A_{21}, A_{22}, \ldots, A_{2N}, \ldots A_{Q1} \ldots A_{QN}\right) \tag{1}$$

The *X*-parameters matrix is the major and key numeric relationships in the function F_{pm}. The NVNA used for the testing of nonlinear device was developed by the Agilent Technologies a few years ago, and the *X*-parameters could be obtained easily from the tested results. The equation for *X*-parameters with single signal is described as given below:

$$[B]_{(\text{response})} = [X][A]_{(\text{stimulus})} \tag{2}$$

$$B_{pm} = X^F_{pm}\left(|A_{(11)}|\right) + \sum_{qn,qn\neq(1,1)}^{QN} X^S_{pm,qn}\left(|A_{(11)}|\right)P^{m-n}A_{qn}$$

$$+ \sum_{qn,qn\neq(1,1)}^{QN} X^T_{pm,qn}\left(|A_{(11)}|\right)P^{m+n}\,\text{conj}\left(A_{qn}\right) \tag{3}$$

where $X^S_{pm,qn}(\cdot)$ and $X^T_{pm,qn}(\cdot)$ are the real and imaginary parts of *X*-parameters, respectively, providing the contribution of signal at input port q with nth harmonic to the signal at output port p, mth harmonic. $X^F_{pm}\left(|A_{11}|\right)$ is the component of the output due to the input signal (A_{11}). So it is only related to the receive port-harmonic pm. A_{qn} is the incident wave at port q, harmonic n and B_{pm} is the response wave at port p, harmonic m. P is defined as $e^{j\phi\,(A11)}$, where $\phi\,(A_{11})$ is the phase of A_{11}. X^F, X^S, and X^T parameters can be directly picked up from the measured results of NVNA.

With the same principle, a two-tone model, for example, that describes an amplifier or mixer can be defined as:

$$B_{P,[nm]} = X^{F}_{P,[nm]}|A_{p1,[1,0]}|,\ |A_{p2,[0,1]}|P^{n}_{[1,0]}P^{m}_{[0,1]}$$

$$+\sum_{q;j,k} X^{S}_{P,[nm];q,[j,k]}|A_{p1,[1,0]}|,\ |A_{p2,[0,1]}|P^{n-j}_{[1,0]}P^{m-k}_{[0,1]}A_{q,[j,k]}$$

$$+\sum_{q;j,k} X^{T}_{P,[nm];q,[j,k]}|A_{p1,[1,0]}|,\ |A_{p2,[0,1]}|P^{n+j}_{[1,0]}P^{m+k}_{[0,1]}\mathrm{conj}\ (A_{q,[j,k]}) \tag{4}$$

For $p_1 = 1$ and $p_2 = 1$, Equation (4) describes an amplifier with a two-tone stimulus at the input port 1. In this case, the port index p of the responsive wave B would go from 1 to 2. The large-signal operating point is specified by the magnitudes of the two input tones.

3. Extracting Volterra series representation from the *X*-parameters matrix

As a common mathematics tool, Volterra series model has definite physical meaning and can embody the essential characteristics of weakly nonlinear system [6,7]. Volterra series representation for a general physical system with $x(t)$ as the input excitation and $y(t)$ as the output response is given as:

$$y(t) = y_1[x(t)] + y_2[x(t)] + y_3[x(t)] + \cdots + y_n[x(t)] + \cdots \tag{5}$$

$$y_n[x(t)] = \frac{1}{n!}\int_{-\infty}^{\infty}\cdots\int_{-\infty}^{\infty} h_n(\tau_1,\ldots\tau_n)\ x_1(t-\tau_1)\ \ldots\ x_n(t-\tau_n)\,d\tau_1\ldots d\tau_n \tag{6}$$

where $y_n[x(t)]$ is the contribution of nth order series. $h_n(\tau_1,\ldots,\tau_n)$ is the nth order Volterra kernel function in time domain which needs to be identified.

For those weakly nonlinear circuits excited by small signals, usually only the first three or four terms are retained. The nonlinearity can be approximated by squared and cubed components [8]. The squared and cubed products in the nonlinearity give rise to harmonic and inter-modulated components. Using Volterra series, closed form expressions of the different distortion components can be obtained. This helps the designer in understanding the circuit more deeply. The nth order frequency response function of the kernel function h_n can be obtained by Fourier transform:

$$H_n(\omega_1,\ldots,\omega_n) = \int_{-\infty}^{\infty}\cdots\int_{-\infty}^{\infty} h_n(\tau_1,\ldots,\tau_n)\ \prod_{i=1}^{n} e^{-j\omega_i\tau_i}d\tau_1\ldots d\tau_n \tag{7}$$

Take a two-tone excitation as an example:

$$x(t) = A_1e^{j\omega_1 t} + A_2e^{j\omega_2 t} \tag{8}$$

The response frequency components are shown as given below (n) up to 3rd harmonic:

$$y_1(t) = \int_{-\infty}^{\infty} h_1(u_1)\left[A_1e^{j\omega_1(t-u_1)} + A_2e^{j\omega_2(t-u_1)} + A_1e^{-j\omega_1(t-u_1)} + A_2e^{-j\omega_2(t-u_1)}\right]du_1 \tag{9}$$

$$y_2(t) = \frac{1}{2!}\int_{-\infty}^{\infty}\int_{-\infty}^{\infty} h_2(u_1,u_2)\left[A_1e^{j\omega_1(t-u_1)} + A_2e^{j\omega_2(t-u_1)} + A_1e^{-j\omega_1(t-u_1)} + A_2e^{-j\omega_2(t-u_1)}\right] \times \left[A_1e^{j\omega_1(t-u_2)} + A_2e^{j\omega_2(t-u_2)} + A_1e^{-j\omega_1(t-u_2)} + A_2e^{-j\omega_2(t-u_2)}\right]du_1du_2 \quad (10)$$

$$y_3(t) = \frac{1}{3!}\int_{-\infty}^{\infty}\int_{-\infty}^{\infty}\int_{-\infty}^{\infty} h_3(u_1,u_2,u_3) \times \left[A_1e^{j\omega_1(t-u_1)} + A_2e^{j\omega_2(t-u_1)} + A_1e^{-j\omega_1(t-u_1)} + A_2e^{-j\omega_2(t-u_1)}\right] \times \left[A_1e^{j\omega_1(t-u_2)} + A_2e^{j\omega_2(t-u_2)} + A_1e^{-j\omega_1(t-u_2)} + A_2e^{-j\omega_2(t-u_2)}\right] \times \left[A_1e^{j\omega_1(t-u_3)} + A_2e^{j\omega_2(t-u_3)} + A_1e^{-j\omega_1(t-u_3)} + A_2e^{-j\omega_2(t-u_3)}\right]du_1du_2du_3 \quad (11)$$

Substitute Equation (7) into Equations (9), (10), and (11):

$$y_1(t) = \frac{A_1}{2}H_1(\omega_1)\ e^{j\omega_1t} + \frac{A_2}{2}H_1(\omega_2)\ e^{j\omega_2t} + \text{ conjugate terms} \quad (12)$$

$$y_2(t) = \frac{A_1^2}{2}H_2(\omega_1,-\omega_1) + \frac{A_2^2}{2}H_2(\omega_2,-\omega_2) + \frac{A_1^2}{4}H_2(\omega_1,\omega_1)\ e^{j2\omega_1t} + \frac{A_2^2}{4}H_2(\omega_2,\omega_2)\ e^{j2\omega_2t} + \frac{A_1A_2}{2}H_2(\omega_1,\omega_2)\ e^{j(\omega_1+\omega_2)t} + \frac{A_1A_2}{2}H_2(\omega_1,-\omega_2)\ e^{j(\omega_1-\omega_2)t} + \text{ conjugate terms} \quad (13)$$

$$y_3(t) = \left[\frac{3A_1^3}{8}H_3(\omega_1,\omega_1,-\omega_1) + \frac{3A_1A_2^2}{8}H_3(\omega_1,\omega_2,-\omega_2)\right]e^{j\omega_1t} + \left[\frac{3A_2^3}{8}H_3(\omega_2,\omega_2,-\omega_2) + \frac{3A_1^2A_2}{8}H_3(\omega_1,-\omega_1,\omega_2)\right]e^{j\omega_2t} + \frac{A_1^3}{8}H_3(\omega_1,\omega_1,\omega_1)\ e^{j3\omega_1t} + \frac{A_2^3}{8}H_3(\omega_2,\omega_2,\omega_2)\ e^{j3\omega_2t} + \frac{3A_1^2A_2}{8}H_3(\omega_1,\omega_1,\omega_2)\ e^{j(2\omega_1+\omega_2)t} + \frac{3A_1^2A_2}{8}H_3(\omega_1,\omega_1,-\omega_2)\ e^{j(2\omega_1-\omega_2)t} + \frac{3A_1A_2^2}{8}H_3(\omega_1,\omega_2,\omega_2)\ e^{j(\omega_1+2\omega_2)t} + \frac{3A_1A_2^2}{8}H_3(-\omega_1,\omega_2,\omega_2)\ e^{j(2\omega_2-\omega_1)t} + \text{ conjugate terms} \quad (14)$$

where the conjugate term is the conjugate part of each frequency component which falls in the negative frequency axis.

As the amplitude of input $x(t)$ increasing, the magnitude of higher order components will increase more quickly than the lower order components. Equations (12)–(14) indicate that the

multi-tone excitation generates several combinational tones in the response series in addition to the fundamental frequencies. Truncating the high-order components until $y_3(t)$ and combining the same frequency components, response amplitudes of various fundamental and combinational tones in frequency domain can be expressed as (taking $\omega_1,\ 2\omega_1,\ \omega_2,\ 3\omega_2,\ 2\omega_2+\omega_1$ for example):

$$Y(\omega_1) = A_1 H_1(\omega_1) + \frac{3A_1^3}{4} H_3(\omega_1,\omega_1,-\omega_1) + \frac{3A_1A_2^2}{4} H_3(\omega_1,\omega_2,-\omega_2); \tag{15a}$$

$$Y(2\omega_1) = \frac{A_1^2}{2} H_2(\omega_1,\omega_1); \tag{15b}$$

$$Y(\omega_2) = A_2 H_1(\omega_2) + \frac{3A_2^3}{4} H_3(\omega_2,\omega_2,-\omega_2) + \frac{3A_2A_1^2}{4} H_3(\omega_1,-\omega_1,\omega_2); \tag{15c}$$

$$Y(3\omega_2) = \frac{A_2^3}{4} H_3(\omega_2,\omega_2,\omega_2); \tag{15d}$$

$$Y(2\omega_2+\omega_1) = \frac{3A_2^2A_1}{4} H_3(\omega_1,\omega_2,\omega_2); \tag{15e}$$

Before the advent of PHD model and *X*-parameters, in order to get the numeric relationships of each frequency component at different ports, we need a large amount of measurement to get enough testing points. Although the Volterra kernel functions can be supposed as symmetry which are independent of arrangement as Equation (16), the testing work is still very onerous for common testing apparatus.

$$h_3(\tau_1,\tau_2,\tau_3) = h_3(\tau_1,\tau_3,\tau_2) = \ldots = h_3(\tau_2,\tau_3,\tau_1) = h_3(\tau_3,\tau_2,\tau_1) \tag{16}$$

Now, the advent of *X*-parameters matrix changes the awkward application of Volterra series. As a many-to-many parameters matrix, *X*-parameters describe the relationships of each fundament and combinational frequency component at each port. As a result, the kernel functions can be extracted based on the numeric relationships. For example, the contributions of the stimulative signals ω_1 and ω_2 at input port to the response frequency components ω_2 and $2\omega_2+\omega_1$ at the output port can be extracted from the *X*-parameters matrix and the value of kernel function at each frequency point can be calculated as:

$$H_3(\omega_1,\omega_2,\omega_2) = \frac{4}{3A_1A_2^2} \cdot \frac{Y(2\omega_2+\omega_1)}{X(\omega_1)X(\omega_2)X(\omega_2)} \tag{17a}$$

$$H_1(\omega_2) = \frac{Y(\omega_2)}{A_2 \cdot X(\omega_2)} \tag{17b}$$

where $Y(\cdot)$ is the power values of response frequency. $X(\omega_1)$ and $X(\omega_2)$ are the frequency domain expressions of $e^{j\omega 1t}$ and $e^{j\omega 2t}$. Be aware that the $H_1(\omega_2)$ is calculated based on the first-order measured data in order to avoid the influence of high-order terms ($H_1(\omega_{2,}-\omega_{2,}\omega_2)$, $H_1(\omega_{1,}-\omega_{1,}\omega_2)$). It is the same principle to the calculation of $H_1(\omega_1)$.

To conclude, the procedure of extracting the kernel functions is described as given below:

(1) First, the database with a wealth amount of information is setup according to the measured *X*-parameters data. The order of signal in the measurement depends on the application. Usually, 3rd is used as the highest order.
(2) For a specific predication of the frequency property, the correlative data are picked up from the database as the base of the calculation. If there is no direct measured data, the average of the most nearest data is used as the base.
(3) After getting the correlative data, the numeric relationships between the each frequency component of the response and the stimulative signals can be obtained. According to the calculation formulas as Equation (4), the value of output power value Y and then H at each concrete frequency point can be calculated as Equation (17). So curves of H can be depicted, and the functions can be achieved by using the curve fitting method.
(4) According to the kernel functions, the value of H at arbitrary frequency point can be calculated and multiplied with the magnitudes of stimulative signals, so the variation of output power with the change of input power can be obtained. As a result, the output performance of each frequency component can be predicated and the characteristics in time domain can also be calculated by inverse Fourier transform.

4. Validation of the method

A GaN HEMT power amplifier module (NPT25015) as shown in Figure 1 was measured by the NVNA provided by Agilent Technologies with two-tone stimulus [9–11]. The voltages of gate and drain were set to −1.38 V and 28 V, respectively [12,13]. The tested ranges of the two stimulative signals ω_1 and ω_2 were listed in the Table 1. The order of harmonic and

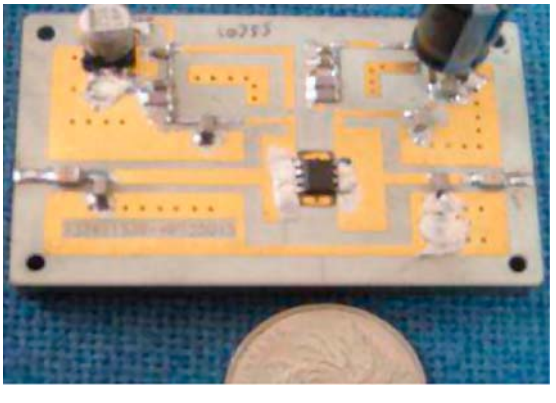

Figure 1. The power amplifier module for measurement in the validation.

Table 1. The measured range of the power amplifier.

	Frequency (MHz)			Input power (dBm)		
	Start	Step	Stop	Start	Step	Stop
ω_1	705	10	995	−10	1	10
ω_2	710	10	990	−10	1	10

inter-modulated wave was set to 3 and the measured X-parameters matrix of the amplifier was written into the MDIF file, based on which the database was established. Compared with common testing apparatus, the total tested points decreased from 4,604,040 to 383,670 with about 91.7% decline of the testing workload. Because the independent variables in Volterra series are the fundamental frequencies ω_1 and ω_2, the harmonic and inter-modulated components at input port in the X-parameters must be neglected. Fortunately, this omission barely influences the calculated results because of the very small contributions to the response compared to fundamental frequencies. In order to make the verification result clearer and the predicated procedure more concise, one stimulus signal ω_1 was fixed and another signal ω_2 varied in the following calculation. The ω_1 was arbitrarily set at 850 MHz with the input power of 10 dBm. Another frequency ω_2 varies from 710 to 990 MHz (except for 850 MHz) with the input power increased from 0 to 15 dBm. Since there were no direct measured data for ω_1 at 850 MHz, the measured data of ω_1 at 845 and 855 MHz were averaged and used as the basic measured data in the predication. According to the basic data, the output power and the value of the kernel function H at each frequency point of the response could be calculated. Then the curves of H vs. the variation of the frequency ω_2 could be described, and the kernel functions can be obtained by using the method of curve fitting. Taking the ω_2 and 2 $\omega_2 + \omega_1$ as an example, the value of H at each frequency point can be calculated by using Equation (17), and the fitting functions for kernel function H were both cubic polynomial models as shown in Figure 2. The output performance of the amplifier can be predicated based on the kernel functions. The predicted results of power and frequency characteristics of the power amplifier were partly shown in the following content because of the limited space.

In the calculation, ω_1 was set to 850 MHz with 10 dBm input power and the frequency of ω_2 was variable with 3 dBm input power. As shown in Figure 2, the value of H at each frequency point was calculated according to X-parameters. The method of curve-fitting equation was used to obtain the function of H. Equations (18) and (19) were corresponding to 2 $\omega_2 + \omega_1$ and ω_2, respectively. Both of the fitting functions were cubic polynomial models. However, the fitting function was not invariable. The type of fitting functions should be adapted to the curve. If one function could not describe the whole curve, separate functions could be chosen.

$$H_3(\omega_{1,}\omega_{2,}\omega_2) = (-6.137e-6) \times \left(\frac{\omega_2}{2\pi}\right)^3 + 0.01767 \times \left(\frac{\omega_2}{2\pi}\right)^2 - 17.24 \times \left(\frac{\omega_2}{2\pi}\right) + 5778 \tag{18}$$

$$H_1(\omega_2) = (-8.652e-7) \times \left(\frac{\omega_2}{2\pi}\right)^3 + 0.002369 \times \left(\frac{\omega_2}{2\pi}\right)^2 - 2.223 \times \left(\frac{\omega_2}{2\pi}\right) + 734.7 \tag{19}$$

After obtaining the fitting functions, the output characteristics were calculated and compared with the measured data. Some representative frequency components were selected as an example as shown in Figures 3 and 4.

In Figure 3, ω_1 was set to 850 MHz with 10 dBm input power and ω_2 variable from 710 to 990 MHz with 3 dBm input power. As shown in the chart, the predicated results by using Volterra series agreed well with the practically measured data.

The values of H at 845 MHz (ω_2) were calculated based on the kernel functions, and the variations of output power with the increase of input power (ω_2) were predicted as shown in

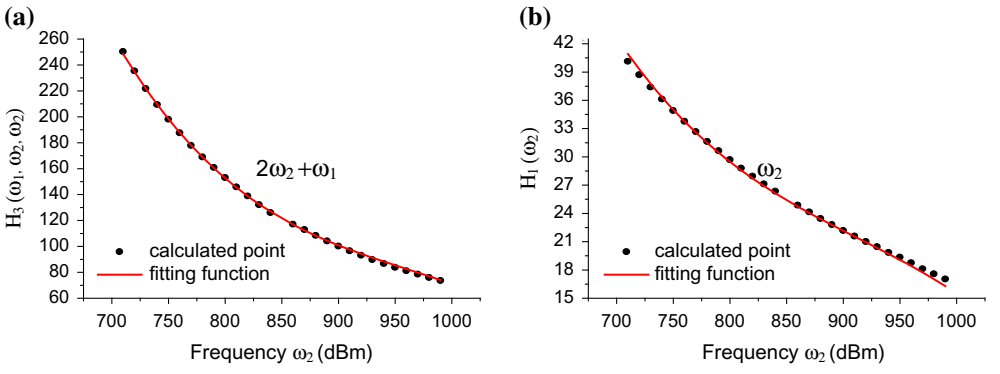

Figure 2. The values of H vs. the variation of frequency ω_2.

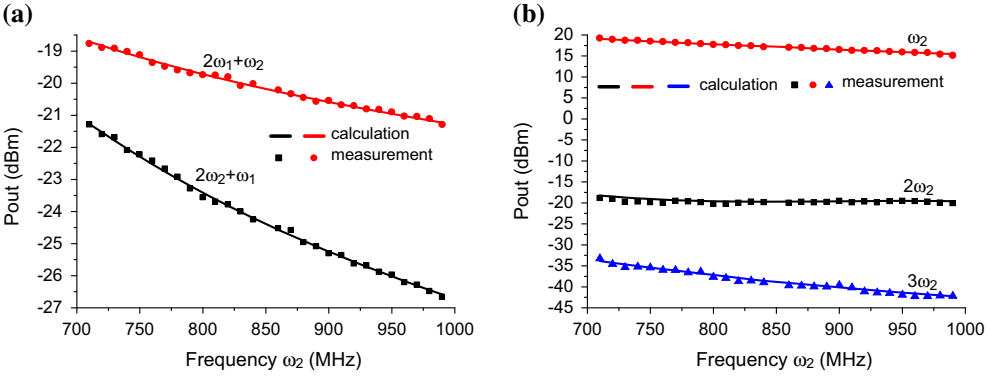

Figure 3. The comparisons of output characteristics between calculated data and measured results.

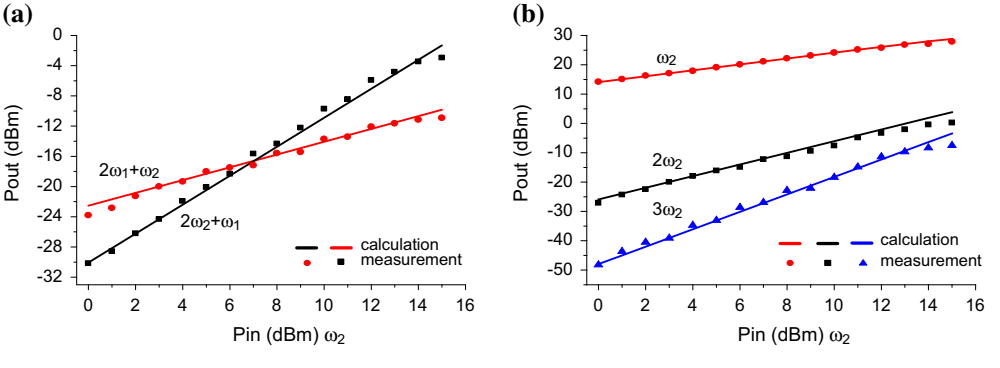

Figure 4. The comparisons of output power vs. input power between calculated data and measured results (the input power of ω_2 was increased from 0 to 15 dBm).

Figure 4 and (ω_1 was also set to 850 MHz with 10 dBm. Due to the weak nonlinearity, the second and third terms in formula (15b) were very small and the compression of output power was not dramatic. The compared results indicated that the prediction based on Volterra series had a high accuracy.

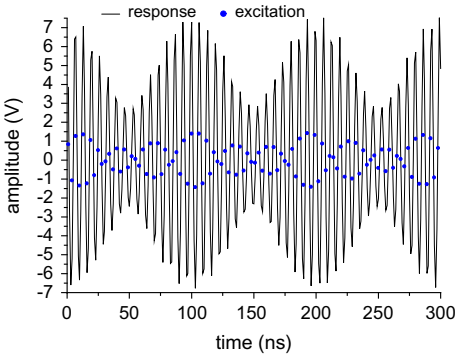

Figure 5. The waveforms of excitation and response in time domain (ω_1 was 850 MHz with 10 dBm input power and ω_2 was 840 MHz with 3 dBm input power).

Figure 5 describes the waveforms of the excitation and response signals based on calculation which contain 2 frequency components (ω_1 and ω_2) and 12 frequency components ($\omega_1,\ \omega_2,\ 2\omega_1,\ 2\omega_2,\ 3\omega_1,\ 3\omega_2,\ \omega_1-\omega_2,\ \omega_1+\omega_2,\ 2\omega_1-\omega_2,\ 2\omega_2-\omega_1,\ 2\omega_1+\omega_2,\ 2\omega_2+\omega_1$),, respectively. It indicated that the difference between the two waveforms was very small except amplitude due to the weak nonlinear effects.

5. Conclusion

The *X*-parameters matrix is used to extract kernel functions of Volterra series firstly in this paper. It is shown that due to the powerful function in the description of nonlinear systems, the numeric relationships between each response frequency component and input fundamental frequency component can be easily obtained by using *X*-parameters. Moreover, the *X*-parameters measurement greatly simplifies the testing work and improves the accuracy of the test results. As a result, the kernel functions of Volterra series in frequency domain can be achieved easily by fitting the concrete point. The comparisons of the calculated data and measured results show that *X*-parameters can be used to extract the kernel functions of Volterra series successfully and conveniently. The predicted data based on this Volterra series representation agree well with the measured results. The proposed approach is useful for accurate and fast modeling of weakly nonlinear modern microwave devices.

References

[1] Sabah C. Multi-resonant metamaterial design based on concentric V-shaped magnetic resonators. J. Electromagnet. Waves Appl. 2012;26:1105–1115.
[2] Wang R, Xu J, Wei CL, Wang M-Y, Zhang X-C. Improved extraction of coupling matrix and unloaded *Q* from *S*-parameters of lossy resonator filters. Prog. Electromagn. Res. 2011;120:67–81.
[3] Volterra V. Theory of functionals and of integral and integro-differential equations. Mineola (NY): Dover Publications; 1959.
[4] Root DE, Verspecht J, Sharrit D, Wood J. Broad-band poly-harmonic distortion behavioral models from fast automated simulations and large signal vectorial network measurements. IEEE Trans. Microw. Theory Tech. 2005;53:3656–3664.
[5] Verspecht J, Root DE. Polyharmonic distortion modeling. IEEE Microw. Mag. 2006 Jun;7(3):44–57.
[6] Schetzen M. The Volterra and Wiener theories of nonlinear system. New York (NY): John Wiley and Sons; 1980.
[7] Sen SG. Analysis of high frequency plane wave transmission into a double negative cylinder by the modified Watson transformation and debye series expansion: first term of the Debye series. Prog. Electromagn. Res. 2011;112:379–414.

[8] Gifford SJ. Estimation of second and third order frequency response functions using truncated models. Mech. Syst. Signal Process. 1997;11:219–228.
[9] Zarifi D, Abdolali A, Soleimani M, Nayyeri V. Inhomogeneous planar layered chiral media: analysis of wave propagation and scattering using Taylor's series expansion. Prog. Electromagn. Res. 2012;125:119–135.
[10] Li S, Tang B, Liu Y, Li S, Yu C, Wu Y. Miniaturized dual-band matching technique based on coupled-line transformer for dual-band power amplifiers design. Prog. Electromagn. Res. 2012;131:195–210.
[11] Wong S-K, Kung Wai Lee F, Maisurah S, Osman MNB. A wimedia compliant cmos RF power amplifier for ultra-wideband (UWB) transmitter. Prog. Electromagn. Res. 2011;112:329–347.
[12] Sang L, Xu Y, Cao Rui, Guo Y, Xu R-M. Modeling of gan hemt by using an improved K-nearest neighbors algorithm. J. Electromagnet. Waves Appl. 2011;25:949–959.
[13] Wu Y, Liu Y, Li S, Li S. A novel high-power amplifier using a generalized coupled-line transformer with inherent DC-block function. Prog. Electromagn. Res. 2011;119:171–190.